Absorption spectrum of doped highly mismatched alloys

Hassan Allami[1] and Jacob J. Krich[1,2]

[1]*Department of Physics, University of Ottawa, Ottawa, Ontario K1N 6N5, Canada*
[2]*Nexus for Quantum Technologies, University of Ottawa, Ottawa, Ontario K1N 6N5, Canada*

Highly mismatched alloys are a class of semiconductor alloys with large electronegativity differences between the alloying elements. We predict that the absorption spectrum due to transitions between the split bands of a doped highly mismatched alloy with a conduction band anticrossing shows qualitative features revealing the fractional distribution of states in the split bands and providing valuable insight into their electronic structure. Our prediction is based on the analysis of the joint densities of states for both direct and indirect transitions between the split bands. In particular, we predict a peak near the absorption edge, which arises due to the suppression of direct transitions at large momenta. As a result of the suppression of direct transitions, indirect transitions dominate the spectrum away from the edge of absorption. We present analytic forms of the near-absorption-edge and large-energy behaviors of the spectra, comparing them with the asymptotic forms of absorption from a single deep impurity level.

I. INTRODUCTION

Semiconductor alloys where the electronegativity or size of the alloying elements significantly differs are called highly mismatched alloys (HMA's). The hallmark of HMA's, as in the prototypical case of GaAsN, is a band gap that changes with alloying in a way that cannot be explained with a simple bowing parameter [1], a feature that found many applications in making various optoelectronic devices [2,3]. According to the band anticrossing (BAC) model, the large decrease in the valence-to-conduction band gap with alloying is associated with a second band gap that opens between two split bands E_- and E_+. According to the BAC, these split bands represent the hybridization of localized states from the alloying element with the conduction band of the host semiconductor (see Fig. 1) [4]. When the localized states hybridize with a single conduction band (CB) of the host, the gap opens by splitting the CB into two split bands, E_- and E_+. In such HMA's with a CB anticrossing, the splitting can generate a narrow intermediate band E_- in the original band gap of the host. The presence of the narrow band makes HMA's a candidate for implementing intermediate band solar cells [5–12], which have the potential to break the Shockley-Queisser limit on solar cell efficiency [13].

An impurity-averaged Green's function approach [14] can be used to show that the two BAC bands share each **k** state in the Brillouin zone. That is, while the E_- and E_+ bands have a clear dispersion with **k**, they do not hold as many electrons as a band in a crystalline semiconductor. We refer to this phenomenon as the fractional state distribution in the split bands. In a previous work, we showed that this fractional distribution can manifest itself in plasmonic properties of HMA's when doped [15], allowing for the possible realization of low-frequency lossless plasmonics [16]. The Green's function approach continues to prove fruitful in studying the electronic structure of HMA's [17]. Here, we show that the fractional

distribution produces a divergence in the joint density of states between the E_- and E_+ bands, which should be visible in the absorption spectrum of doped HMA's, adding to our growing knowledge of these alloys [18]. There has been success in doping HMA's so the E_- band is partially full at equilibrium [19], but the absorption spectra of doped HMA's have not been studied. Although the absorption spectrum between the two split bands of an HMA is crucial for example in operation of intermediate band solar cells, there is not much known about it.

In this work, we predict the absorption spectra of doped highly mismatched alloys with a conduction band anticrossing. We show that the fractional distribution of states in the split bands of this entire class of material leads to asymptotic behavior of the spectra near the absorption edge that are different from the spectra from isolated impurities in semiconductors. We show that at higher energies the behavior of the absorption spectrum is similar to that from a single deep impurity level, but the differences near the absorption edge are particularly dramatic when the localized states are inside the CB. We argue that such spectra carry definitive signatures for the fractional distribution of states in HMA's.

In general, the band-to-band absorption spectrum of a material, in the single-particle picture, is determined by the joint density of states (jDOS) and the effective transition matrix element $M(E)$. The jDOS is a measure of the number of pairs of occupied and unoccupied states separated by energy E, and $M(E)$ is the average of the dipole transition matrix elements between those pairs of states. It is well known that the variation of jDOS with energy is often the dominant factor in determining the energy profile of the spectrum [20–24] and even where the effects of $M(E)$ make quantitative changes, they do not change the overall shape of the absorption profile [25,26]. Especially in the case of dilute alloys and disordered materials such as HMA's, where *ab initio* computation of the matrix element is costly, jDOS is
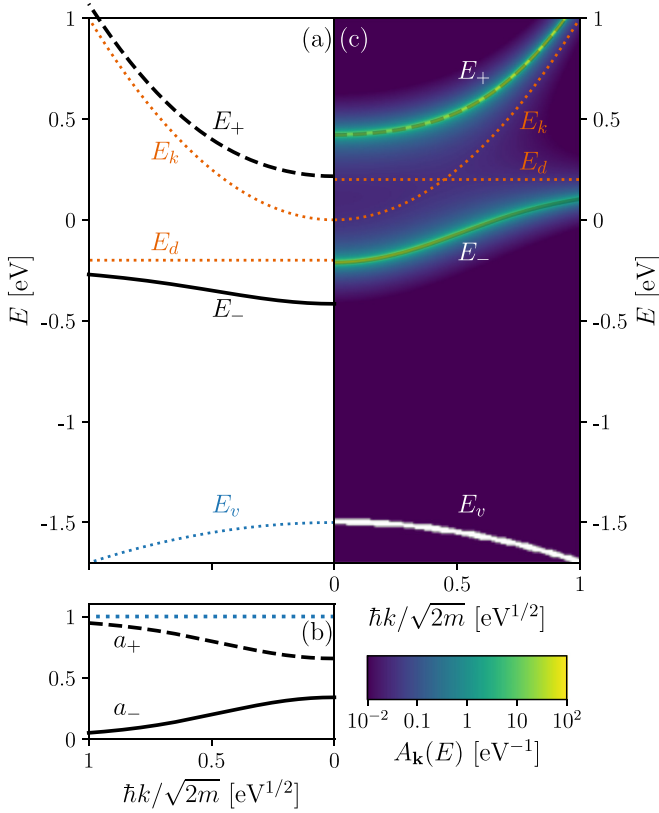
FIG. 1. (a) Band anticrossing bands $E_\pm$ according to Eq. (1), together with a schematic valence band E_v. (b) The corresponding spectral weighting factors $a_\pm$ from Eq. (11), with defect energy $E_d = -0.2$ eV and broadening $\Gamma = 0$. The weight for E_v is constant 1 (dotted blue). (c) Spectral density $A_\mathbf{k}(E)$ for $E_d = 0.2$ eV and $\Gamma = 100$ meV from Eq. (7). Note the logarithmic colorscale. For reference, $E_\pm$ according to Eq. (1) are also plotted in (c). In both cases $V = 3$ eV and $x = 1\%$. The spectral density for E_v is an ideal delta function, shown by excluding its location from the plot.

often used to explain the qualitative features of the absorption profile [27–29].

By contrast, in transitions from a single deep impurity level to a continuum, the localized wave function can be easily approximated, and the matrix element shows a strong k dependence, which results in the suppression of higher-energy transitions above the absorption edge [30,31]. Since HMA's form when there are many such impurity states (though not necessarily deep in the band gap), such impurities are a natural point of comparison. In the HMA case, the wave functions, and thus the matrix elements, in both E_+ and E_- bands are not easily determined, but we show that the k-conserving jDOS itself encodes the same suppression of absorption at higher energies, which is attributed to matrix element effects in the isolated-impurity case. The result is that at higher energies, the HMA jDOS is similar to the absorption spectrum from deep impurity levels. Near the absorption onset, however, the fractional state density of the HMA's when the localized states are in the CB of the host gives them a diverging absorption edge rather than the square-root onset in the impurity case. We derive the jDOS directly from the Green's function and include the effects of partial state occupation due to finite

temperature by considering the equilibrium Fermi distribution. We present results at 300 K, but the predicted features are qualitatively unchanged as long as the temperature is small compared to the bandwidth of the E_- band.

Throughout the paper we focus on the absorption due to the transitions between the split bands and neglect the transitions from the valence bands. In typical HMA's, including the ones considered in Sec. III, the energy range of transitions between the split bands is smaller than the fundamental gap between the valence bands and E_-. Beyond the single-particle picture, bonding between electron-hole pairs may result in excitonic peaks also near the edge of absorption. Although our model does not go beyond the single-particle picture, we comment in Sec. III that the peak that we predict is easily distinguishable from possible excitonic peaks by varying the doping level.

II. ABSORPTION SPECTRUM AND JOINT DENSITY OF STATES

While the BAC model [4] is very successful in describing the energy levels in the band structure of HMA's, it is quiet about how the propagating states are distributed among these energies. The BAC energy levels are reproduced by an impurity-averaged Green's function in the coherent potential approximation (CPA) introduced by Wu *et al.* [14]. The spectral density derived from that Green's function describes how the hybridized propagating states of HMA's are distributed at each $\mathbf{k}$. Here we show how the fractional state distribution leads to qualitative features in the absorption spectrum of doped HMA's.

A. HMA's distribution of states and the absorptivity

According to the BAC model [4], large differences in the electronegativities of the mismatched elements compared to the host leads to the formation of localized states with energy E_d. These localized states hybridize with the propagating states of the unalloyed host, which have dispersion $E_\mathbf{k}$, resulting in the emergence of two new split bands with dispersions

$$E_\pm = \tfrac{1}{2}(E_\mathbf{k} + E_d \pm \sqrt{(E_\mathbf{k} - E_d)^2 + 4V^2 x}), \qquad (1)$$

where V is the coupling energy between the localized and the propagating states, and x is the alloy fraction of the mismatching element (see Fig. 1).

Although Eq. (1) is a great approximation for the energy dispersion of $E_\pm$, the split bands of HMA's are not just two regular bands arising from a periodic potential of a crystal. They are both offspring of the hybridization of a single band with a series of randomly distributed localized states. If we assume that the alloying elements are uniformly distributed, as in the coherent potential approximation [32], we may still use the crystal momentum $\mathbf{k}$ as a good quantum number in an ensemble-average sense. The exact hybridized eigenstates with energy E have a nonzero projection on each $\mathbf{k}$ state. As a result, at each $\mathbf{k}$, there is a distribution $A_\mathbf{k}(E)$, known as the spectral density, that describes the projection of all hybridized states with energy E on the $\mathbf{k}$ states. As we show in Sec. II B, the spectral density $A_\mathbf{k}(E)$ can be broken into two branches, $A_\mathbf{k}^\pm(E)$, corresponding to $E_\pm$.

Now consider a doped HMA where some excess electrons are occupying the $E_\pm$ bands. Under illumination with radiation of frequency ω, suppose we want to calculate transition rates of electrons from E_--energy states to E_+-energy states. Consider **k**-conserving direct transitions, which are normally the strongest band-to-band transitions. To find the direct transition amplitudes, at each **k** we must know how many states there are in each band. For example, the density of spin-up electrons at **k** belonging to the E_- band is $\int dE\, A_{\mathbf{k}}^-(E) f_E$, instead of the usual $f_{E_-(\mathbf{k})}$, where $f_E = (e^{(E-\mu)/T} + 1)^{-1}$ is the Fermi distribution at temperature T and chemical potential μ.

The usual discussion of absorptivity in semiconductors begins from a Fermi's golden rule analysis, generally called the Kubo-Greenwood formula [20]. The absorptivity for photons with energy E is controlled most importantly by the joint density of states (jDOS) at energy E, which describes the number of pairs of states in the lower- and higher-energy bands that are separated by energy E. Calculating the jDOS, we need to take $A_{\mathbf{k}}$ into account, as it carries important information about how the propagating states are distributed at each **k**. For direct absorption processes, the relevant jDOS is $D_j(E)$, which includes only pairs of states with the same momentum **k**. For indirect absorption processes, the relevant jDOS is $\rho_j(E)$, which includes all pairs of states separated by energy E, regardless of **k**. For both contributions to the optical absorption, there is a matrix element that must be averaged over all contributing initial and final states. The result is that the absorptivity due to direct processes $\alpha_d \propto |M_D|^2 D_j(E)/E$ and the absorptivity due to indirect processes $\alpha_i \propto |M_\rho|^2 \rho_j(E)/E$, where M_D and M_ρ are the averaged matrix elements. In general for band-to-band absorptions, the matrix elements M_D and M_ρ also depend on E, but since many different transitions contribute to the same energy, their E dependence is weak and is not usually the dominant factor in determining the general profile of α [20,21]. For an isolated deep impurity level, the localized wave function has weak overlap with high-k continuum states, giving a matrix element that decays with increasing E [30,31]. The average Green's function approach includes this same overlap reduction in the jDOS itself.

We consider both direct momentum-conserving transitions between E_- and E_+ and indirect transitions that do not conserve momentum. Indirect transitions are typically made possible through phonon exchange, but in the case of an alloy are also possible without phonons, due to the disorder. Absorption and emission of phonons that make the indirect transitions possible bring a small shift to the edge of the optical absorption spectrum, which we neglect as it does not affect the qualitative features we describe here. Therefore, we can approximate the absorption profile as [20]

$$\alpha(E) \propto \frac{D_j(E) + v\rho_j(E)}{E}, \tag{2}$$

where $v = |M_\rho|^2/|M_D|^2$ is a volume scale of the system, which we treat as a free parameter.

Calculating the jDOS's for HMA's must account for the distribution of electrons at different energies according to $A_{\mathbf{k}}^\pm(E)$, which is averaged over the alloy disorder. Assuming that E_- and E_+ are statistically uncorrelated, we can write the direct and indirect jDOS as

$$D_j(E) = \frac{1}{\mathcal{V}} \int dE_1 dE_2 \sum_{\mathbf{k}} A_{\mathbf{k}}^-(E_1) A_{\mathbf{k}}^+(E_2) f_{E_1}\big(1 - f_{E_2}\big) \\ \times \delta(E_2 - E_1 - E), \tag{3}$$

$$\rho_j(E) = \frac{1}{\mathcal{V}^2} \int dE_1 dE_2 \sum_{\mathbf{k}\mathbf{k}'} A_{\mathbf{k}}^-(E_1) A_{\mathbf{k}'}^+(E_2) f_{E_1}\big(1 - f_{E_2}\big) \\ \times \delta(E_2 - E_1 - E), \tag{4}$$

where $\mathcal{V}$ is the volume of the system. In Appendix A we use supercell tight-binding models to show that correlation effects appear to be small for the interband jDOS. Comparing the dimension of Eqs. (3) and (4) also shows why the ratio $v = |M_\rho|^2/|M_D|^2$ has the dimension of volume. Note that we neglect the spin degree of freedom, unless otherwise mentioned, as it does not affect the shape of $\alpha(E)$. The presence of $A_{\mathbf{k}}^\pm$ in the jDOS expressions produces the signatures of the fractional state distribution of $E_\pm$ in the absorption spectrum of a doped HMA.

B. HMA spectral density and resulting joint density of states

We now discuss how the distribution of states in HMA's, given by $A_{\mathbf{k}}(E)$, generates qualitative features in α according to Eq. (2). We begin by deriving $A_{\mathbf{k}}(E)$. Based on Anderson's impurity model [33], Wu *et al.* built an average Green's function for electrons in the conduction bands of an HMA [14]

$$G(E, \mathbf{k}) = \left[E - E_{\mathbf{k}} - \frac{V^2 x}{E - E_d + i\Gamma} \right]^{-1}, \tag{5}$$

which successfully recovers the spectrum of the BAC model. The new parameter $\Gamma = \pi \beta V^2 \rho_0(E_d)$ determines the broadening of the Green's function's spectral density, where ρ_0 is the unperturbed density of propagating states in a unit cell and has dimension of inverse energy. In what follows we consider a generic case where $E_{\mathbf{k}}$ is a parabolic conduction band and all energies are measured from its edge. Therefore, for instance, $\Gamma \to 0$ for $E_d < 0$, as $\rho_0 = 0$ below the conduction band edge.

While Eq. (5) and the BAC model contain the same energy spectrum in the limit that $\Gamma \to 0$, even in that limit the spectral density $A_{\mathbf{k}}(E) = -\mathrm{Im}[G(E, \mathbf{k})]/\pi$ contains information about what fraction of an electron can be in each of the states. Since there is less than one alloying atom per unit cell of the host crystal, the E_- and E_+ bands can not each hold as many electrons as the original $E_{\mathbf{k}}$ band.

We can divide $A_{\mathbf{k}}(E)$ into two pieces, corresponding to $E_\pm$ as

$$A_{\mathbf{k}}(E) = A_{\mathbf{k}}^+(E) + A_{\mathbf{k}}^-(E) = \frac{1}{\pi} \sum_{s=\pm} \mathrm{Im}\left[\frac{\tilde{a}_s}{E - \tilde{E}_s} \right], \tag{6}$$

where, including the effects of Γ, the dispersion of Eq. (1) is generalized to

$$\tilde{E}_\pm = \tfrac{1}{2}\left(E_{\mathbf{k}} + \tilde{E}_d \pm \sqrt{(E_{\mathbf{k}} - \tilde{E}_d)^2 + 4V^2 x}\right), \tag{7}$$

TABLE I. Asymptotic behavior of the contribution of the direct and indirect transitions to $E\alpha(E)$ in $\Gamma \to 0$ limit at the absorption edge and for large E, for the cases of negative and positive E_d, compared with the case of deep impurity [31]. E_D is the edge of direct transitions, and E_ρ is the edge of indirect transitions.

	Direct		Indirect	
	Edge	Large E	Edge	Large E
$E_d > 0$ HMA	$1/\sqrt{E - E_D}$	$E^{-3/2}$	$E - E_\rho$	$\sqrt{E}$
$E_d < 0$ HMA	$\sqrt{E - E_D}$	$E^{-3/2}$	$E - E_\rho$	$\sqrt{E}$
Deep impurity (allowed) [31]	$\sqrt{E - E_D}$	$E^{-3/2}$	$\sqrt{E - E_\rho}$	$\sqrt{E}$

with $\widetilde{E}_d = E_d + i\Gamma$, and the generalized weight factors are

$$\widetilde{a}_\pm = \pm \frac{V^2 x}{(\widetilde{E}_+ - \widetilde{E}_-)(\widetilde{E}_\pm - E_{\mathbf{k}})}. \quad (8)$$

A realization of $A_{\mathbf{k}}(E)$ with a finite Γ is shown in Fig. 1(c). Note that most of the spectral weight is near the BAC bands, but the weight spreads out to nearby energies, as well.

When $\Gamma \to 0$, Eq. (7) reduces to Eq. (1) and the spectral density reduces to two delta functions at $E_\pm$:

$$\lim_{\Gamma \to 0} A_{\mathbf{k}}(E) = a_+ \delta(E - E_+) + a_- \delta(E - E_-), \quad (9)$$

with

$$a_\pm = \pm \frac{V^2 x}{(E_+ - E_-)(E_\pm - E_{\mathbf{k}})}, \quad (10)$$

which we derived previously to show how the state distribution in HMA's affects their plasmonic properties [15]. The weight factors $a_\pm$ in Eq. (11) are positive numbers smaller than 1, representing the share of a single $\mathbf{k}$ state in each of $E_\pm$. A realization of $a_\pm$ is shown in Fig. 1(b) in a case with $E_d < 0$ where $\Gamma \to 0$.

In the limit $\Gamma \to 0$, we can find analytic forms for Eqs. (3) and (4). These results are exact for the $E_d < 0$ case. While the analytic forms are not exact when $E_d > 0$, the analytic results from the $\Gamma \to 0$ limit provide useful insight to the behavior of D_j and ρ_j with finite Γ as well. We derive these analytic forms and their implications for finite Γ cases in Appendix B. Table I summarizes the qualitative results, showing the scaling of D_j and ρ_j with energy near their respective energy onset and at large energy.

We observe that similar to the case of a single deep impurity level [30,31], the direct E_- to E_+ optical transition is suppressed at higher energy, showing the same $E^{-3/2}$ behavior. The E_- states at high k have mostly localized character, and as a result the spectral density a_- is small, as is visible in Fig. 1(b). Since there is little weight in these large-k states, $D_j(E)$ is suppressed, producing a peak in the direct optical absorption spectrum. Further, away from the edge of absorption $\rho_j \sim \sqrt{E}$, as one would expect from transitions from a single impurity state to a parabolic continuum.

However, the edge of absorption is different from the case of absorption from isolated deep impurity levels. The case where the localized states are in the CB of the host has no analogy in the isolated-level context. In that case the edge of direct absorption is dramatically different, with a divergence

at the absorption edge rather than a square-root onset. Near $k = 0$ the set of localized states forms a flat band. When $E_d > 0$ the flat band crosses the CB of the host, which leads to $E_+ - E_-$ acquiring a minimum at a finite k. In Appendix B we show how this finite-k minimum leads to the divergence of D_j at the edge of absorption, as shown in Table I. The asymptotic behavior of indirect transitions at the absorption edge is also different from the case of a single deep impurity level, as we discuss in Appendix B and show in Table I. That difference from square root to linear onset may be harder to detect, especially in the case of $E_d > 0$, where the finite Γ smears the absorption edge.

The finite Γ in the case of $E_d > 0$ turns the divergence into a peak the width of which is controlled by Γ. Hence, this peak also provides a practical way to estimate Γ, which is otherwise a difficult quantity to measure. In the case of $E_d < 0$ the peak's width is controlled by $|E_d|$, as we show in Appendix B. The presence of the peak in the direct optical absorption is the most significant feature of the absorption spectra, and according to Eq. (2) should be visible in plots of $E\alpha(E)$, which is proportional to the jDOS according to Eq. (2).

In Eq. (2), we do not know the ratio of indirect to direct matrix elements v, but in general in semiconductors indirect processes are weaker than direct ones, as they need to couple phonons in to the system. However, since HMA's are random alloys and not crystalline semiconductors, it is possible that momentum conservation between states holds less strongly than in standard semiconductors, which would increase the magnitude of the indirect matrix element compared to the direct matrix element in the absorptivity, increasing the ρ_j contribution with respect to the D_j contribution. In any case, our key results do not depend on the precise value of v, as they are the consequence of qualitatively different behavior of D_j and ρ_j. Indirect processes are most important at energies where the direct processes are suppressed, and we predict that in the form of the E_- to E_+ absorption spectrum the same pattern will hold. We predict that since D_j decays as $E^{-3/2}$ for large E, while ρ_j grows as $\sqrt{E}$, then for large enough v the indirect transitions will dominate the large-E part of the E_- to E_+ absorption spectrum. Reference [9] on the transient absorption spectrum of HMA's invoked indirect transitions to explain their observed high-energy absorption. Here we provide a firm theoretical basis for indirect transitions dominating direct transitions at higher energy. The indirect absorption edge occurs at lower energy than the direct absorption edge, allowing indirect absorption also to dominate for energies below the direct absorption edge. This effect is most noticeable when $E_d < 0$ since the direct absorption spectrum is broadened by Γ when $E_d > 0$.

All of these features are the direct consequence of the fractional distribution of states in HMA's, and detecting them in experiments would be a good validation test for the theory. Notice that, given the generality of $E_{\mathbf{k}}$ in Eq. (5), this theory can easily extend to capture the effects of nonparabolicity as well. To apply the theory to valence band HMA's, where the impurity levels cross multiple bands, an extended formulation of the average Green's function is needed. This extended version should effectively capture the hybridization of impurity levels with the multiple bands.

Parameters	$y = 0$	$y = 1$
E_d (eV)	−0.27	0.38
V (eV)	2.8	2.2
m (m_e)	0.117	0.09

III. EXPERIMENTAL SIGNATURES

We illustrate the predictions for the signatures of E_- to E_+ optical absorption by considering HMA's from the ZnCdTeO family, where the BAC parameters have been estimated [34,35]. $Zn_{1-y}Cd_yTe_{1-x}O_x$ is a II-VI quaternary HMA in which ZnCdTe forms the standard semiconductor and oxygen plays the role of mismatching element. It has been the subject of extensive studies and used as an HMA of choice in making devices [8,19,34,36–40]. We choose ZnCdTeO for our case study because there have been successful attempts in doping the E_- band with chlorine donors [19]. Moreover, controlling the Cd concentration allows for sweeping E_d. BAC parameters for the ternary end-point alloys are given in Table II, which shows that by increasing Cd fraction, E_d moves from negative to positive. For all x, y, the fundamental band gap between the valence bands and E_- stays well above 1 eV [35], so the transitions from the valence bands do not affect the absorption profile in the range of our concern. For the sake of demonstration, Table II shows the results for the two ternary end points ZnTeO and CdTeO, but tuning the Cd fraction allows realization of any E_d between −0.27 and 0.38 eV, along with changes in V and m.

Even for two parabolic valence and conduction bands $\alpha(E)$ shows a peak due to the factor of E in the denominator of Eq. (2). Instead, we consider $E\alpha$ which is proportional to the jDOS and reveals the signature of the fractional distribution of states in the split bands of HMA's. While experimentally we generally specify doping level n, the absorption depends most directly on the chemical potential appearing in the Fermi function f_E. We relate them using

$$n = \frac{2}{\mathcal{V}} \int dE \sum_{\mathbf{k}} A_{\mathbf{k}}(E) f_E, \tag{11}$$

where the factor of 2 accounts for spin degeneracy. In Fig. 2 we plot $E\alpha$ at $T = 300$ K for doped ZnTeO (top) and CdTeO (bottom), according to Eq. (2), for two doping levels. For the case with a lower doping level, we also show the contributions of direct and indirect transitions to $E\alpha$ separately (shaded blue). We use $v = 10$ nm^3, chosen strong enough so that ρ_j visibly dominates D_j away from the edge of absorption. To calculate D_j and ρ_j for CdTeO we used the full form in Eqs. (3) and (4). For ZnTeO, since $E_d < 0$ and $\Gamma \to 0$, we use Eq. (B2) to compute D_j and Eq. (B3) to calculate ρ_j.

The absorption peak from the direct transitions is clear for both materials in Fig. 2. We can see that the CdTeO ($E_d > 0$) peak is narrower than the one in ZnTeO ($E_d < 0$), which we expect as the $E_d > 0$ cases have peak widths controlled by Γ while the $E_d < 0$ have them controlled by $|E_d|$, as discussed
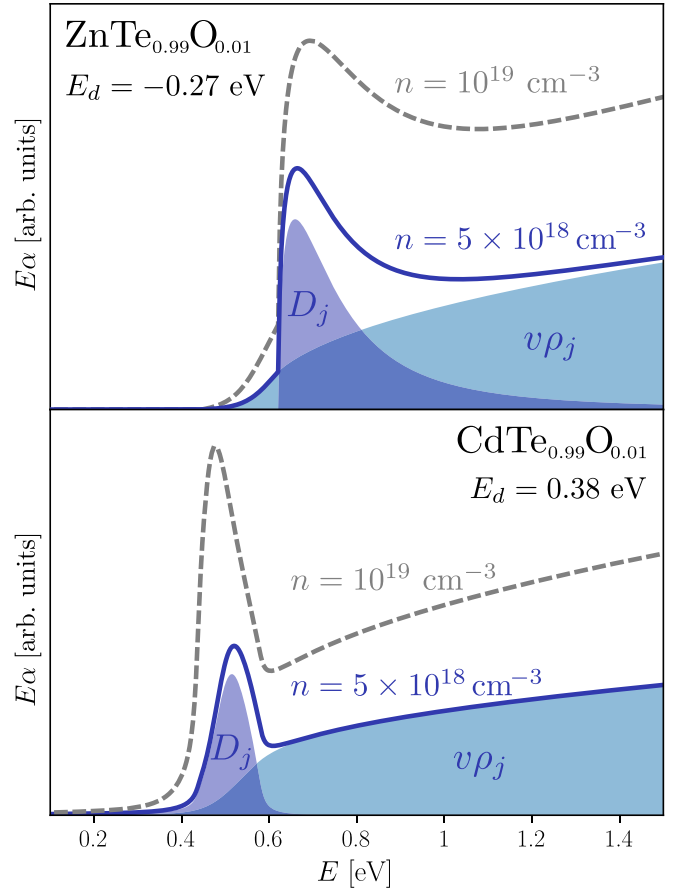

FIG. 2. E_- to E_+ optical absorption $E\alpha$ at $T = 300$ K for ZnCdTeO alloys with two doping levels, $n = 5 \times 10^{18}$ cm^{-3} (solid blue) and $n = 10^{19}$ cm^{-3} (dashed gray). The separate contributions of direct and indirect transitions also shown for the lower doping level (shaded blue), according to Eq. (2), where $v = 10$ nm^3 is used for all cases. (Top) $ZnTe_{1-x}O_x$, with $x = 1\%$, and BAC parameters listed in Table II, for which $\Gamma \to 0$. (Bottom) $CdTe_{1-x}O_x$, with $x = 1\%$, BAC parameters listed in Table II, and $\Gamma = 10$ meV for broadening.

in Appendix B. And since $\Gamma \propto \sqrt{E_d}$ when $E_d > 0$, we expect to see narrower peaks for cases with smaller $|E_d|$.

Figure 2 also demonstrates that the indirect transitions dominate at large E in both material systems, due to the decaying large-E tail of D_j. Also, the indirect transitions become available at lower energy, as they are not limited by conservation of momentum, but this effect is only visible for the $E_d < 0$ case where $\Gamma \to 0$ does not smear out the edge of absorption. In this case, the different behavior of the edge from the case of a single deep impurity can be confirmed. Since Γ being zero in the $E_d < 0$ case gives sharper features to α, we also expect the edge of D_j to be visible as a kink in the absorption in these cases, as shown for ZnTeO.

To show the effects of increased filling of the E_- band, we include two doping levels in Fig. 2, $n = 5 \times 10^{18}$ cm^{-3} (solid blue) and $n = 10^{19}$ cm^{-3} (dashed gray), for both ZnTeO and CdTeO. It is clear that the mentioned features of $E\alpha$, the peak and the dominance of indirect transitions at large E, are present at both doping levels. It is possible that excitonic peaks, which generally occur at energies just below the jDOS

onset [41], could be confused for the peak that we predict. The evolution of the peak as a result of increasing doping also provides a way to distinguish it from a possible excitonic peak. In a doped HMA, both screening from carriers in the E_- band and the disordered potential should suppress excitons [42], so we expect the possible excitonic peak to diminish at higher doping. As Fig. 2 shows, the peak that we expect to be visible in $E\alpha$ naturally grows stronger at higher doping, making it distinguishable from an excitonic one.

It is worth noting that although according to Ref. [19] achieving chlorine concentration up to and even higher than 10^{20} cm^{-3} is possible, it is not clear what portion of the dopants are electrically active. Especially as our model with weighted bands shows, E_- has a relatively small maximum capacity for carrying excess electrons. For instance, for ZnTe$_{1-x}$O$_x$ and CdTe$_{1-x}$O$_x$ with $x = 1\%$ used for plotting Fig. 2, the maximum capacity of E_- is about 5×10^{19} cm^{-3} and 6×10^{19} cm^{-3}, respectively. Electrically active doping above those levels will populate the E_+ band, with changes to the E_- to E_+ absorption spectrum, similar to the Moss-Burstein shift [43,44].

In the ZnCdTeO system, the typical frequency range for E_- to E_+ absorption is around 0.1–1 eV, or a wavelength of 1–10 μm. These spectra can be observed with Fourier-transform infrared (FTIR) or other techniques appropriate for these long wavelengths. We look forward to seeing the results of such experiments, to see if they confirm our theoretical predictions. We believe experimental results for the absorption spectrum of doped HMA's will be instrumental in understanding their interesting electronic structure better.

APPENDIX A: CORRELATION IN THE JOINT DENSITY OF STATES

In the main text, we calculate the joint densities of states from the disorder-averaged single-particle densities of states. This procedure neglects correlations between the energies in the $E_\pm$ bands. In particular, allowing an overline to indicate disorder averaging, Eqs. (3) and (4) use the uncorrelated average $\overline{A}_{\mathbf{k}}(E_1)\overline{A}_{\mathbf{k}'}(E_2)$ rather than the true physical quantity, which has $\overline{A_{\mathbf{k}}(E_1)A_{\mathbf{k}'}(E_2)}$. Here we use explicit calculations of eigenenergies in a simple-cubic tight-binding (TB) model with explicit impurities to show that correlations in the jDOS do not appear to be significant, and we expect the analytic calculations of the main text to provide good representations of the true jDOS.

We use a simple-cubic TB model because the parabolic model underlying the Green's function in Eq. (5) is not conducive to explicit calculation. This Green's function originates in the coherent potential approximation (CPA) applied to a parabolic-band model hybridizing with local disorder, with k-independent coupling coefficient. To make explicit calculations, we here use a simple-cubic TB model with nearest-neighbor hopping, with randomly located impurity sites that have onsite energies of $-\delta$ while host sites have

onsite energy δ. This model is fully determined by the half-bandwidth D of the host band structure δ and the impurity fraction x. We align these bands with the BAC bands, determined by V, E_d, and x, by noting that the bottom of the unperturbed host band is at $\delta - D$, implying $E_d = D - 2\delta$.

We calculate the one-particle DOS in this simple-cubic model both using the CPA and by explicit diagonalization of realizations with disorder, with the results compared to the DOS produced by Green's function of Eq. (5), which we refer to as BAC DOS, in Fig. 3(a). The CPA calculations use the Python package GFTOOL [45]. We consider CdTe$_{1-x}$O$_x$ with the BAC parameters of Table II, with $x = 1\%$, and adjust D until the DOS of the TB CPA model, suitably shifted and scaled, aligns by eye with the BAC DOS, which occurs with $D = 2.95$ eV and $\delta = (D - E_d)/2 = 1.285$ eV. Using $a_\pm$ in Eq. (10), one can derive an analytical expression for the BAC DOS as

$$\rho_\pm(E) = \frac{1}{\mathcal{V}} \sum_{\mathbf{k}} a_\pm \delta(E - E_\pm)$$

$$= \frac{1}{4\pi^2}\left(\frac{2m}{\hbar^2}\right)^{3/2} \begin{cases} \sqrt{E - \frac{V^2 x}{E - E_d}} & \text{for } E \text{ in } E_\pm, \\ 0 & \text{otherwise.} \end{cases} \quad \text{(A1)}$$

By increasing the size of supercell, we observe that the DOS of the supercell calculations in the E_+ region approaches that of the TB CPA. In the E_- region the bandwidth of the TB CPA and supercell calculations are in agreement, but in supercell calculations the supercell DOS shows a sharp spike in the middle of E_- that persists as the supercell size grows. It appears that the CPA does not capture this feature. The BAC DOS is not expected to agree quantitatively, as it is from a different model, but it is clear that the chosen parameters give good agreement between the BAC model and the energetic positions of the $E\pm$ bands.

We use the supercell spectra to investigate correlation in jDOS. When formulating Eqs. (3) and (4), we assumed that one can first average over an ensemble of realizations to find the DOS of the system before calculating the jDOS as a convolution of the DOS with itself. However, if there exists correlation within the system, this jDOS would differ from the jDOS obtained by convolving the DOS of each disorder realization prior to averaging over all realizations. We express these two distinct procedures for the more straightforward case of indirect jDOS as

$$\rho_j(E) = \int \overline{\rho}(E_1)\overline{\rho}(E_1 + E)f_{E_1}(1 - f_{E_1+E})dE_1, \quad \text{(A2a)}$$

$$\widetilde{\rho}_j(E) = \int \overline{\rho(E_1)\rho(E_1 + E)}f_{E_1}(1 - f_{E_1+E})dE_1, \quad \text{(A2b)}$$

where ρ_j follows our assumption and disregards the correlations, while $\widetilde{\rho}_j$ includes correlations. Setting the chemical potential in the gap between E_- and E_+, as depicted in the left panel of Fig. 3, we illustrate the insignificance of correlation in the jDOS in the right panels. Figure 3(b) superimposes ρ_j and $\widetilde{\rho}_j$, while Figs. 3(c) and 3(d) show their absolute and relative differences, respectively. Near zero energy in Fig. 3(d), the normalized difference reaches about $\pm 30\%$, which is due to noise, given that the jDOS goes to zero in that region. We find that when μ is located where the DOS is near zero, the
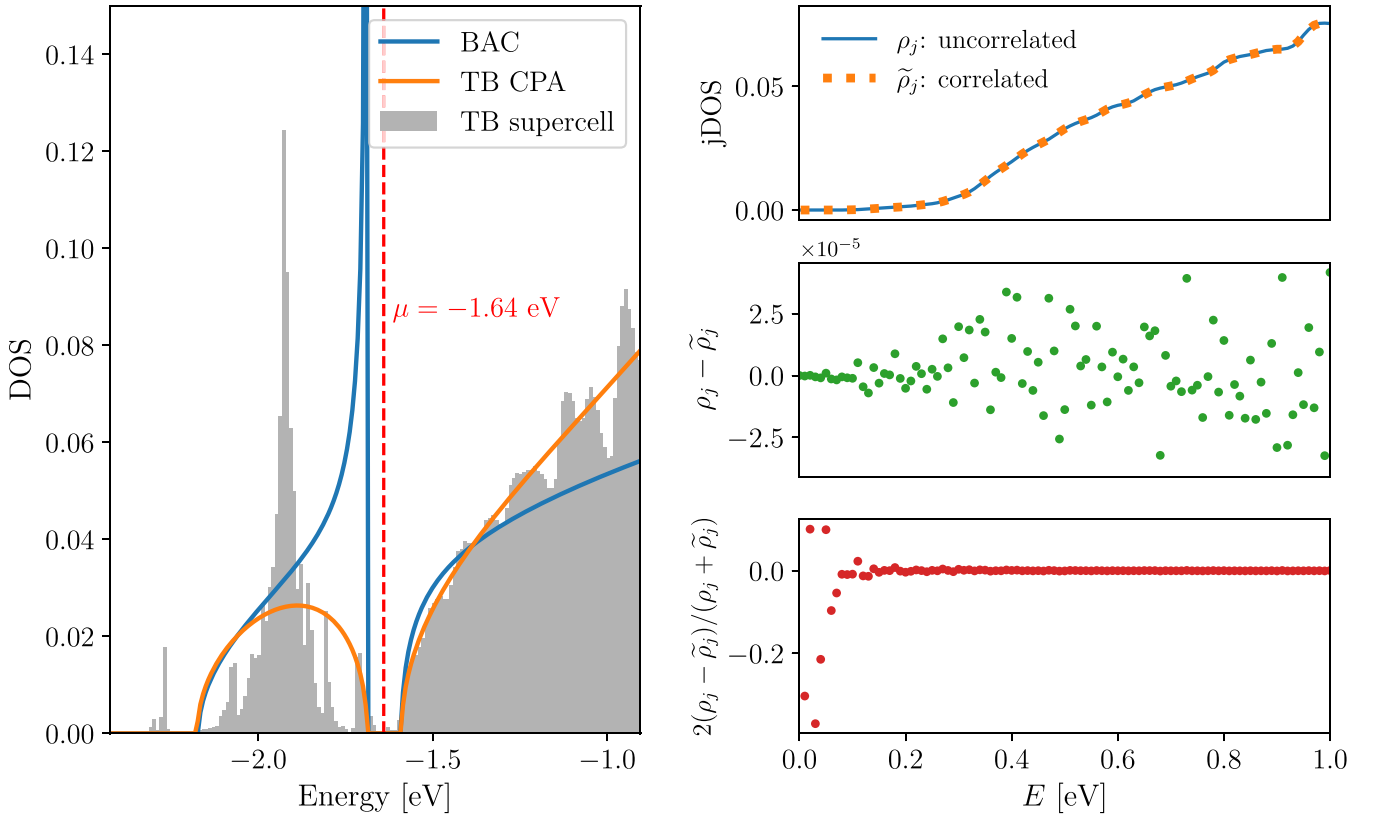
FIG. 3. (a) Density of states (DOS) from three models approximating CdTe$_{1-x}$O$_x$ using parameters in Table II, with $x = 1\%$. Result from the BAC-inspired Green's function (blue), as in the main text, coherent potential approximation (CPA) of simple-cubic tight-binding model (orange), and supercell calculation of 100 realizations of disorder in 30^3-site system (gray), shown as a histogram. The tight-binding parameters are chosen to match the BAC DOS, used for both CPA and supercell calculations. (b) The uncorrelated jDOS ρ_j and the correlated jDOS $\widetilde{\rho}_j$, as expressed in Eq. (A2b), for the supercell model, at zero temperature, with $\mu = -1.64$ eV, as shown in (a) by a dashed vertical line. (c) Absolute difference between ρ_j and $\widetilde{\rho}_j$. (d) Relative difference between ρ_j and $\widetilde{\rho}_j$. Collectively, (b)–(d) demonstrate that correlations in the jDOS between E_- and E_+ are negligible.

relative difference between $\widetilde{\rho}_j$ and ρ_j is only significant near zero energy, where jDOS goes to zero. We also did not observe any significant correlation when the chemical potential was located inside $E_\pm$, with the relative difference between $\widetilde{\rho}_j$ and ρ_j becoming larger than 1% only where the jDOS itself is near zero (not shown).

APPENDIX B: ANALYTIC FORMS AND ASYMPTOTICS OF D_j AND ρ_j

1. Direct joint density of states

Using the sharp $A_{\mathbf{k}}$ in Eq. (9), the E_1 and E_2 integrals in Eq. (3) become trivial. Furthermore, since $E_{\mathbf{k}} = \hbar^2 k^2 / 2m$ is isotropic we can integrate the angles out to obtain a one-dimensional integral

$$
\begin{aligned}
D_j(E) &= \frac{1}{\mathcal{V}} \sum_{\mathbf{k}} a_- a_+ f_{E_-} (1 - f_{E_+}) \delta(E_+ - E_- - E) \\
&= \frac{V^2 x}{2\pi^2} \int_0^\infty \frac{f_{E_-}(1 - f_{E_+})}{(E_+ - E_-)^2} \delta(E_+ - E_- - E) k^2 \, dk.
\end{aligned}
\tag{B1}
$$

Note that the factor of $a_- a_+$ originates from the nontrivial spectral density of the HMA, and this extra factor produces

the $(E_+ - E_-)^2$ in the denominator of Eq. (B1), which makes D_j decay for large E, similar to the decay for the case of a deep impurity level [30,31].

When $E_d \leqslant 0$, $E_+ - E_-$ has a minimum at $k = 0$ with the value $\sqrt{E_d^2 + 4V^2 x}$. Therefore, the argument of the delta function in Eq. (B1) has a zero if $E \geqslant \sqrt{E_d^2 + 4V^2 x}$, determining the edge of D_j. Carrying out the delta function integral is straightforward and gives

$$
\begin{aligned}
D_j(E) &= \left(\frac{2m}{\hbar^2}\right)^{3/2} \frac{V^2 x \sqrt{E_d + \sqrt{E^2 - 4V^2 x}}}{4\pi^2 E \sqrt{E^2 - 4V^2 x}} f_{\widehat{E}_-} (1 - f_{\widehat{E}_+}) \\
&\quad \times \Theta\left(E - \sqrt{E_d^2 + 4V^2 x}\right),
\end{aligned}
\tag{B2}
$$

where $\widehat{E}_\pm = E_d + \frac{1}{2}(\sqrt{E^2 - 4V^2 x} \pm E)$, and Θ is the unit step function. One can see that the fraction in Eq. (B2) decays as $E^{-3/2}$ for large E (see Table I). Since D_j in Eq. (B2) is positive, continuous, and zero at the edge of direct transitions $E_D = \sqrt{E_d^2 + 4V^2 x}$, it must have a peak. The width of that peak is determined by $|E_d|$. In this case, $D_j(E)$ rises as $\sqrt{E - E_D}$. The peak is visible in the top panel of Fig. 2, which is plotted for an HMA with $E_d < 0$.

When $E_d > 0$, $E_+ - E_-$ has a minimum at $k = \sqrt{2mE_d}/\hbar$ with value $2V\sqrt{x}$, which leads to a van Hove singularity at $E_D = 2V\sqrt{x}$ with the same form as the van Hove singularities in 1D materials with parabolic bands. That is, for $E \geqslant E_D$, $D_j(E) \sim 1/\sqrt{E - E_D}$, which is divergent at the onset. This one-dimensional-like form arises from the finite-k^2 volume element when $E_+ - E_-$ reaches its minimum value in Eq. (B1). This divergence does not have a counterpart in the case of single deep impurity state [30,31]. The van Hove singularity arises only when $A_\mathbf{k}$ is sharp as in Eq. (9), in the limit of $\Gamma \to 0$ (see Table I). But when $E_d > 0$, Γ is nonzero and broadens $A_\mathbf{k}^\pm$. Finite Γ turns the divergence of D_j into a peak with a width determined by Γ. The peak is visible in the bottom panel of Fig. 2, which shows an HMA with $E_d > 0$.

The other consequence of $E_+ - E_-$ having a minimum at finite k is that the argument of the delta function in Eq. (B1) has two zeros when $2V\sqrt{x} < E < \sqrt{E_d^2 + 4V^2x}$, which leads to two separate contributions to the integral. However, for large E, where the finite Γ effect is also unimportant, there is only one contribution to the integral in Eq. (B1). Therefore, the large-E behavior of D_j is the same for both positive and negative E_d (see Table I).

2. Indirect joint density of states

To evaluate the non-k-conserving density of states in Eq. (4), after integrating $\mathbf{k}$ and $\mathbf{k}'$ out, we obtain a convolution between the DOS of E_- and E_+ bands as

$$\rho_j(E) = \int dE_1 dE_2 \rho_-(E_1)\rho_+(E_2) f_{E_1}(1 - f_{E_2})\delta(E_2 - E_1 - E)$$

$$= \int dE_1 \rho_-(E_1)\rho_+(E_1 + E) f_{E_1}(1 - f_{E_1+E}), \qquad \text{(B3)}$$

which we can compute by employing the analytical expression given in Eq. (A1). The edge of ρ_j is at the minimum gap between the E_+ and E_- bands, given by $E_\rho = \frac{1}{2}(\sqrt{E_d^2 + 4V^2x} - E_d)$, and it rises linearly, unlike the case of a single deep impurity level (see Table I). The difference occurs because here we have the convolution of two DOS associated with $E_\pm$ rather than the transitions from one single state to the DOS of a continuum. In the limit of large E, the E dependence in Eq. (B3) comes from ρ_+, which goes as $\sqrt{E}$, as can be seen from Eq. (A1). Therefore, ρ_j shows $\sqrt{E}$ behavior for large E, similar to absorption due to transitions from an impurity state to a parabolic continuum. The more important implication of this result is that since D_j decays as $E^{-3/2}$, the indirect transitions can dominate the large-E part of the E_- to E_+ absorption spectrum, where the direct transitions are suppressed. Figure 2 shows this effect away from the edge of absorption.

Lastly, we note that nonzero Γ smears out the edge of ρ_j and has no significant effect on its large-E behavior.

[1] M. Weyers, M. Sato, and H. Ando, Red shift of photoluminescence and absorption in dilute GaAsN alloy layers, Jpn. J. Appl. Phys. **31**, L853 (1992).

[2] S. Nakamura and M. R. Krames, History of gallium–nitride-based light-emitting diodes for illumination, Proc. IEEE **101**, 2211 (2013).

[3] D. Friedman, J. Geisz, S. Kurtz, and J. Olson, 1-eV solar cells with GaInNAs active layer, J. Cryst. Growth **195**, 409 (1998).

[4] W. Shan, W. Walukiewicz, J. W. Ager, E. E. Haller, J. F. Geisz, D. J. Friedman, J. M. Olson, and S. R. Kurtz, Band anticrossing in GaInNAs alloys, Phys. Rev. Lett. **82**, 1221 (1999).

[5] N. López, L. A. Reichertz, K. M. Yu, K. Campman, and W. Walukiewicz, Engineering the electronic band structure for multiband solar cells, Phys. Rev. Lett. **106**, 028701 (2011).

[6] N. Ahsan, N. Miyashita, M. M. Islam, K. M. Yu, W. Walukiewicz, and Y. Okada, Two-photon excitation in an intermediate band solar cell structure, Appl. Phys. Lett. **100**, 172111 (2012).

[7] M. Welna, M. Baranowski, W. M. Linhart, R. Kudrawiec, K. M. Yu, M. Mayer, and W. Walukiewicz, Multicolor emission from intermediate band semiconductor ZnO$_{1-x}$Se$_x$, Sci. Rep. **7**, 44214 (2017).

[8] T. Tanaka, K. M. Yu, Y. Okano, S. Tsutsumi, S. Haraguchi, K. Saito, Q. Guo, M. Nishio, and W. Walukiewicz, Improved open-circuit voltage and photovoltaic properties of ZnTeO-based intermediate band solar cells with n-type ZnS layers, IEEE J. Photovoltaics **7**, 1024 (2017).

[9] J. N. Heyman, A. M. Schwartzberg, K. M. Yu, A. V. Luce, O. D. Dubon, Y. J. Kuang, C. W. Tu, and W. Walukiewicz, Carrier lifetimes in a *III-V*-N intermediate-band semiconductor, Phys. Rev. Appl. **7**, 014016 (2017).

[10] K. Zelazna, R. Kudrawiec, A. Luce, K.-M. Yu, Y. J. Kuang, C. W. Tu, and W. Walukiewicz, Photoreflectance studies of optical transitions in GaNPAs intermediate band solar cell absorbers, Sol. Energy Mater. Sol. Cells **188**, 99 (2018).

[11] J. N. Heyman, E. M. Weiss, J. R. Rollag, K. M. Yu, O. D. Dubon, Y. J. Kuang, C. W. Tu, and W. Walukiewicz, THz transient photoconductivity of the III-V dilute nitride GaP$_y$As$_{1-y-x}$N$_x$, Semicond. Sci. Technol. **33**, 125009 (2018).

[12] A. Qayoom, S. Yagi, and H. Yaguchi, Nitrogen concentration dependence of two-step photocurrent generation by below-gap excitation in GaPN alloys, Phys. Status Solidi B **261**, 2300369 (2024).

[13] A. Luque and A. Martí, Increasing the efficiency of ideal solar cells by photon induced transitions at intermediate levels, Phys. Rev. Lett. **78**, 5014 (1997).

[14] J. Wu, W. Walukiewicz, and E. E. Haller, Band structure of highly mismatched semiconductor alloys: Coherent potential approximation, Phys. Rev. B **65**, 233210 (2002).

[15] H. Allami and J. J. Krich, Plasma frequency in doped highly mismatched alloys, Phys. Rev. B **103**, 035201 (2021).

[16] H. Allami and J. J. Krich, Lossless plasmons in highly mismatched alloys, Appl. Phys. Lett. **120**, 252102 (2022).

[17] M. Seifikar, E. P. O'Reilly, and S. Fahy, Band dispersion, scattering rate, and carrier mobility using the poles of Green's function for dilute nitride alloys, J. Appl. Phys. **135**, 045704 (2024).

[18] W. Walukiewicz and J. M. O. Zide, Highly mismatched semiconductor alloys: From atoms to devices, J. Appl. Phys. **127**, 010401 (2020).

[19] T. Tanaka, K. Matsuo, K. Saito, Q. Guo, T. Tayagaki, K. M. Yu, and W. Walukiewicz, Cl-doping effect in $ZnTe_{1-x}O_x$ highly mismatched alloys for intermediate band solar cells, J. Appl. Phys. **125**, 243109 (2019).

[20] M. P. Marder, Optical properties of semiconductors, in *Condensed Matter Physics* (Wiley, Hoboken, NJ, 2010), Chap. 21, pp. 633–657.

[21] S. Kasap, C. Koughia, J. Singh, H. Ruda, and S. O'Leary, Optical properties of electronic materials: Fundamentals and characterization, in *Springer Handbook of Electronic and Photonic Materials*, edited by S. Kasap and P. Capper (Springer, Boston, 2007), Chap. 3, pp. 47–77.

[22] R. L. Hartman, Energy dependence of indirect optical absorption in semiconductors, Phys. Rev. **127**, 765 (1962).

[23] P. K. Chakraborty, L. J. Singh, and K. P. Ghatak, Simple theory of the optical absorption coefficient in nonparabolic semiconductors, J. Appl. Phys. **95**, 5311 (2004).

[24] M. Alouani, L. Brey, and N. E. Christensen, Calculated optical properties of semiconductors, Phys. Rev. B **37**, 1167 (1988).

[25] W. B. Jackson, S. M. Kelso, C. C. Tsai, J. W. Allen, and S.-J. Oh, Energy dependence of the optical matrix element in hydrogenated amorphous and crystalline silicon, Phys. Rev. B **31**, 5187 (1985).

[26] S. K. O'Leary, S. R. Johnson, and P. K. Lim, The relationship between the distribution of electronic states and the optical absorption spectrum of an amorphous semiconductor: An empirical analysis, J. Appl. Phys. **82**, 3334 (1997).

[27] J. Hwang and J. D. Phillips, Band structure of strain-balanced GaAsBi/GaAsN superlattices on GaAs, Phys. Rev. B **83**, 195327 (2011).

[28] P. Biswas, R. Atta-Fynn, and S. R. Elliott, Metadynamical approach to the generation of amorphous structures: The case of *a*-Si:H, Phys. Rev. B **93**, 184202 (2016).

[29] S. K. O'Leary, S. Zukotynski, and J. M. Perz, Optical absorption in amorphous semiconductors, Phys. Rev. B **52**, 7795 (1995).

[30] G. Lucovsky, On the photoionization of deep impurity centers in semiconductors, Solid State Commun. **3**, 299 (1965).

[31] J. C. Inkson, Deep impurities in semiconductors. II. The optical cross section, J. Phys. C: Solid State Phys. **14**, 1093 (1981).

[32] R. J. Elliott, J. A. Krumhansl, and P. L. Leath, The theory and properties of randomly disordered crystals and related physical systems, Rev. Mod. Phys. **46**, 465 (1974).

[33] P. W. Anderson, Localized magnetic states in metals, Phys. Rev. **124**, 41 (1961).

[34] T. Tanaka, K. Mizoguchi, T. Terasawa, Y. Okano, K. Saito, Q. Guo, M. Nishio, K. M. Yu, and W. Walukiewicz, Compositional dependence of optical transition energies in highly mismatched $Zn_{1-x}Cd_xTe_{1-y}O_y$ alloys, Appl. Phys. Express **9**, 021202 (2016).

[35] S. Adachi, *Properties of Semiconductor Alloys: Group-IV, III-V and II-VI Semiconductors* (Wiley, Hoboken, NJ, 2005), Chap. 7, p. 150.

[36] T. Tanaka, Y. Nagao, T. Mochinaga, K. Saito, Q. Guo, M. Nishio, K. M. Yu, and W. Walukiewicz, Molecular beam epitaxial growth of ZnCdTeO epilayers for intermediate band solar cells, J. Cryst. Growth **378**, 259 (2013).

[37] T. Tanaka, M. Miyabara, Y. Nagao, K. Saito, Q. Guo, M. Nishio, K. M. Yu, and W. Walukiewicz, Photocurrent induced by two-photon excitation in ZnTeO intermediate band solar cells, Appl. Phys. Lett. **102**, 052111 (2013).

[38] T. Tanaka, S. Kusaba, T. Mochinaga, K. Saito, Q. Guo, M. Nishio, K. M. Yu, and W. Walukiewicz, Molecular beam epitaxial growth and optical properties of highly mismatched $ZnTe_{1-x}O_x$ alloys, Appl. Phys. Lett. **100**, 011905 (2012).

[39] M. Wełna, R. Kudrawiec, Y. Nabetani, T. Tanaka, M. Jaquez, O. D. Dubon, K. M. Yu, and W. Walukiewicz, Effects of a semiconductor matrix on the band anticrossing in dilute group II-VI oxides, Semicond. Sci. Technol. **30**, 085018 (2015).

[40] M. Welna, Ł. Janicki, W. M. Linhart, T. Tanaka, K. M. Yu, R. Kudrawiec, and W. Walukiewicz, Effects of the host conduction band energy on the electronic band structure of ZnCdTeO dilute oxide alloys, J. Appl. Phys. **126**, 083106 (2019).

[41] D. C. Reynolds and T. C. Collins, *Excitons: Their Properties and Uses* (Elsevier, Amsterdam, 2012).

[42] V. L. Bonch-Bruevich and V. D. Iskra, On the theory of the Wannier-Mott excitons in disordered semiconductors, Phys. Status Solidi B **68**, 369 (1975).

[43] E. Burstein, Anomalous optical absorption limit in InSb, Phys. Rev. **93**, 632 (1954).

[44] T. S. Moss, The interpretation of the properties of indium antimonide, Proc. Phys. Soc. B **67**, 775 (1954).

[45] A. Weh and A. Östlin, GfTool 0.11.0 release, Zenodo, https://doi.org/10.5281/zenodo.6507956 (2022).